1 .

Textured dysprosium and gadolinium poles for high-field, short-period hybrid undulators

Alex Murokh[a], Vyacheslav Solovyov[b], Ron Agustsson[a], Finn H. O'Shea[a,c], Oleg Chubar[b], Yung Chen[a], Thomas Grandsaert II[a]

[a] *RadiaBeam Technologies, Inc, 1717 Stewart St., Santa Monica, CA 90404*
[b] *Brookhaven National Laboratory, Upton NY 11973*
[c] *Department of Physics, University of California, Los Angeles, Los Angeles, CA 90095*

Abstract

We discuss the feasibility of enhancement of the gap field in a short-period hybrid undulator by using pole inserts with the saturation inductance B_s, over that of iron, 2 Tesla. Dysprosium metal, with the saturation inductance of 3.4 Tesla below 90 K, and Gadolinium with $B_s = 2.7$ Tesla, appear as a good candidates as the optimized pole material. However, due to the high magnetic anisotropy of Dy, such a high level of magnetization can only be realized when the external field lies in the basal plane. This implies that the pole has to be single-crystalline or highly textured. Considering that growing large, >10 mm, Dy single crystals is difficult, we propose secondary recrystallization as a method to induce the required texture in thin Dy and Gd foils. The textured foils can be stacked to produce pole inserts of the desired geometry and orientation. Results of small-scale processing and magnetic measurements of thin (20-60 microns) foils provide evidence that the required texture quality can be achieved by a relatively simple sequence of heat-treatments and cold rolling. The advantage of textured Dy and Gd poles is demonstrated in a several period test undulator.

Keywords:

1. Introduction

Discovery of high-flux rare-earth-iron-boron permanent magnets in 80s [11] enabled development of short-period, high field undulators. Today, the majority

Email address: oshea@radiabeam.com (Finn H. O'Shea)

of undulators are designed as so-called Halbach arrays [9], of which the hybrid design can be described as a sequence of opposing permanent magnets separated by soft ferromagnetic poles. Combination of Nd-Fe-B permanent magnet with the remnant induction Br = 1.2 T [11] and Vanadium-Permendur [5] poles with the saturation induction $B_s = 2.3$ T, allows achieving 1.3 T peak gap field with a gap-to-period ratio of 0.4. Incremental but steady improvement of the remnant induction, accelerated with the introduction of cryo-cooled Pr-Fe-B magnets [10], raises a question whether iron-based poles are still adequate for the modern high-field, short period undulators.

Dysprosium metal has the saturation inductance of 3.8 T at 4.2 K. Relatively high Curie temperature, 90 K, makes Dy suitable for magnetic applications below 77 K, either as a part of a cryo-cooled permanent magnet array or a superconducting undulator. Rare earth poles made from polycrystalline Holmium and Dysprosium have been used to augment magnetic flux in superconducting magnets [1, 4] and undulators [8]. Due to low magnetic permeability of these poles, a measurable flux gain is possible only in a superconducting system. The field strength in a permanent-magnet system is on the order of 10 kOe, therefore a useful pole should have initial permeability over 10.

Dysprosium has a hexagonal close packed (*hcp*) structure [18], schematically shown in Fig. 1a. This type of structure imposes strong anisotropy on the magnetic properties of the material: dysprosium has very hard direction along [0001] (normal to the basal plane), followed by the moderately hard direction $<10\underline{1}0>$ and easy $<11\underline{2}0>$ directions [2, 6]. A polycrystalline Dy sample, which is comprised of randomly oriented crystallites, would be a very hard ferro-magnet with an apparent saturation in moderate magnetizing fields, $<$10 kOe, well below the saturation induction of the single crystal. To realize the advantage of Dy over a well-established Vanadium-Permendur (V-P) material in a permanent magnet based undulator, one needs a crystallographically oriented Dy pole so that the magnetizing field is directed along the easy axis or, at least, in the basal plane. A straightforward solution would be cutting the pole from a single crystal. However, small size of the available crystals and the expensive equipment involved in the process make this route most likely impractical. Gadolinium metal has an identical *hcp* structure, however it is magnetically softer than Dysprosium. The easy magnetization direction of Gd is tilted at about 30° with respect to the (1000) direction [14]. The disadvantage of Gd is relatively low saturation magnetization, 2.7 T, however higher permeability values can be more readily attained as compared to Dy.

Secondary re-crystallization offers a scalable way to manufacture textured foils of various metals. The process is widely used to induce texture in rolled foils of fcc metals, such as Ni [15], Al, Fe-Si alloys [16]. In the early 1970s Westinghouse research group suggested the secondary re-crystallization process to manufacture large-scale Dy foils [21]. Fig. 1b,c is a simplified illustration of secondary re-crystallization process. A cold-rolled Dy tape is polycrystalline, comprised of small (<100 nm) primary Dy grains, Fig. 1b. Some grains have favorable orientation, with [001] direction parallel to the tape normal and the fast-growth ab-plane parallel to the tape face. The better oriented grains gain a small energetic advantage over other grains, which becomes amplified as the grains start to grow during the subsequent annealing. During the annealing the secondary grains expand rapidly, consuming misoriented primary grains through so-called abnormal grain growth mechanism [12]. At the end of this processing step, only very large (> 10 μm), well-oriented secondary grains remain, Fig. 1c.

In this work we analyze feasibility of using re-crystallized Dy and Gd foils as poles of a cryo-cooled hybrid undulator. We show that secondary re-crystallization can be used to produce textured foils suitable for the pole application.

2. Experiment

2.1. Synthesis of textured Dy and Gd poles

Dysprosium foils were produced by sequential cold rolling of Dy ingots until the foil thickness was reduced to 25 -100 μm. The foils were annealed in vacuum (10^{-6} torr) in a quartz tube furnace at 1100-1200°C for 10-20 min. The tube was evacuated by a diffusion pump with a liquid nitrogen cold trap. The difficulty with annealing dysprosium metal is very high reactivity, which is explained by low free energy of Dy_2O_3. Due to such a low value of free energy, Dy metal can oxidize by reducing quartz to silicon, therefore a very expensive ultra-high vacuum annealing system is typically required. To avoid oxidation of the foils during annealing at relatively low vacuum pressure, they were enclosed in a specially designed molybdenum annealing cell. The cell restricted flow of oxygen to the surface of the Dy foil so that Dy vapor, present at these temperatures, reacted with the entering oxygen creating local ultra-high vacuum environment. As a result the foils had clean and shiny surfaces with only minor surface oxidation. The foil structure was analyzed using a four-circle x-ray diffractometer. Magnetic properties of foils were measured by a superconducting magnetometer in external field up to 7 Tesla.

A laminated piece was assembled by pressing the Dy foils into a 2 mm composite and subsequent annealing of the piece at 1100°C in vacuum. After this treatment the foils fused into a solid block with the density over 98% of bulk Dy. The 12×1.6 mm^2 test poles were machined from the block to exact dimensions of existing V-P poles.

A similar rolling-annealing procedure was employed to manufacture Gd poles.

2.2. Two period undulator testing

The 2-period undulator consisted of a pair of jaws held together by a strong back that serves to both define the magnetic gap and secure the undulator to the test bench. The entire assembly is made out of copper to minimize thermal gradients. The main part of the jaw is a precision-machined block that contains a series of grooves that alternately hold magnets and poles. As the stable magnetic lattice applies a force on the magnets that pushes them into the copper block, no additional restraint of the magnets is necessary. To maximize the thermal contact with the copper structure the grooves are made as deep as possible. The first step in the jaw assembly is placing in the poles and then securing them with the keepers. Next the magnet grooves are coated with thermally conducting cryogenic-compatible grease. The jaw piece and the magnets are cooled to -20°C and the magnets are inserted into the lattice. PrFeB magnets are used, because they do not show a spin axis reorientation (SAR) between 77 K and room temperature, unlike NdFeB magnets [3]. As these magnets have larger remanent field than samarium-cobalt magnets (which also do not show an SAR in the given temperature range), they were chosen to maximize the field applied to the poles. The magnets are cooled before insertion because the magnets see the largest reverse fields during magnet insertion [17]. After the magnets are safely in the lattice, the reverse fields are low enough that the magnets are safe at room temperature. Once the jaws are assembled they are bolted to the copper strong back to define the 2.5 mm gap. The c-axis of the textured dysprosium poles was oriented in the horizontal direction (see Fig. 2). The partially assembled test undulator is shown in Fig. 2a.

A test stand with a small area scanning Hall probe was designed to measure the central magnetic field at cryogenic temperature, Fig. 2b. The entire setup was placed within an insulated enclosure to minimize convective heating. This baseline design was tested with a low temperature thermocouple probe and demonstrated that we could maintain a sufficient LN_2 bath for $\sim$20 minutes.

The test undulator consists of two jaws, each containing 5 poles and 6 magnets; five of the poles in one jaw can be seen in Fig. 2. For each rare-earth material, two measurements of the test undulator are made at 77 K. In the first measurement, all of the poles are V-P and in the second measurement, one of the poles, number 4, in each jaw is replaced with Dy or Gd (see Fig. 2).

3. Results

3.1. Structure and magnetic properties of textured Dy foils

The optical micrograph shown in Fig. 3 is an experimental demonstration of the Dy secondary recrystallization process, schematically illustrated in Fig. 1b and c. One can easily observe large secondary grains forming after annealing of a rolled Dy tape, Fig. 3b.

Fig. 4 compares x-ray diffraction 2θ scans of 60 and 25 μm foils after 10 min anneals at 1000 and 1100°C. Intensity of $(hkil)$ peaks in as-rolled foils is identical to that of a powder, which is an indication of random texture. Annealing at 1000°C produces partial (000l) (c-axis normal to the foil surface) texture. The low quality of the texture is evident from the relatively intense (1013) peak. The (1013) plane is inclined at 15° with respect to (0001), thus presence of an intense (1013) peak is an indication that multiple grains are tilted at >10°. Increasing the annealing temperature up to 1100°C improves the foil texture, which is evident from reduced intensity of the (1013) peak. It is the combination of large compression ratio, that is a result of the rolling, and the annealing cycle that generates the texture, no magnetic field applied during the annealing cycle.

The texture quality is traditionally quantified by broadening of rocking curves across the principal texture directions, typically in-plane and out-of-plane ones. Re-crystallization of Dy foils produced only uni-axial out-of-plane texture; we did not detect any in-plane alignment. This is in contrast with fcc cubic metals, such as Ni, Al or Cu, where sharp in-plane texture is routinely produced by a similar rolling-annealing routine. The out-of-plane texture quality of rolled Dy foils is easily quantified by rocking curve (θ-scan) of Dy (0004) reflection, as shown in Fig. 5 a,b. Due to very large size of the grains (>100 mm, see Fig. 3b) the θ-scans appear as a superposition of sharp reflections from individual Dy grains. The scan is approximated by a Gaussian shown as a solid line. To summarize the texture optimization experiment, we observe the texture quality improve as the annealing temperature is increased up to 1100°C. At this temperature, the optimum annealing time is 20 min, after which the $\delta\theta$ value reached is 4-5° for 25 μm foils and 8-10° for 60 μm foils.

The mechanism of the texture formation can be understood from optical micrographs presented in Fig. 5c,d. Here the same area of a 25 μm thick foil is photographed after 10 and 20 min processing at 1100°C. According to Fig. 5a,b the $\delta\theta$ value drops by a factor of two in this time interval. Two grains, labeled A and B, are outlined for clarity in micrograph (c). After the extra 10 min of annealing, grain A grows from 100 to 400 μm consuming in the process smaller grains, including 30 μm grain B. This process of fast expansion of a few better oriented grains at the expense of smaller, mis-oriented ones explains sharpening of the θ-scan in Fig. 5a,b.

Fig. 6 compares results of magnetization measurements of the textured foils with the single crystal data Behrendt *et al.* [2] and a polycrystalline Dy sample. Magnetic measurements demonstrate large improvements in magnetization over the polycrystalline sample Fig. 6, in particular when a thinner Dy foil (25 μm) was used. The textured foils have lower absolute value of magnetization than [1120] oriented crystal, more important is relatively low value of the initial permeability.

3.2. Structure and magnetic properties of textured Gd foils

Fig. 7 summarizes the results of re-crystallization procedure applied to Gd foils. The results are essentially similar to that of Dy: a (000l) texture formed after a slow annealing at 1100°C. We notice however, that Gd has a stronger oxidation tendency, thus several strong peaks, identified with a '*' in Fig. 7a, are identified as Gd oxide. Nevertheless, the annealed Gd foil surface, shown in Fig. 7b shows relatively clean surface with well-defined secondary grains.

Fig. 8 compares the magnetization curves of polycrystalline Gd and textured 100 mm thick foil at 300, 77 and 4.2 K. Although, gadolinium is a much softer ferro-magnet than dysprosium, still it takes approximately 1 T to saturate a polycrystalline Gd sample at 77 K. Texturing significantly improves permeability by a factor of 5 and increases the saturation moment by 16%.

3.3. Performance of the Dy and Gd poles in undulator array

Fig. 9 shows field scans of the test array with Dy (panel a) and Gd (panel b) at room temperature and 77 K. At room temperature Dy is paramagnetic and Gd has the easy magnetization direction along the c-axis, therefore both Gd and Dy poles perform far worse than V-P. The gap field rises as the Dy pole becomes ferromagnetic at 90 K, eventually outperforming V-P at < 80 K, Fig. 10. In the case of Gd the field improvement is explained by a combination of lower temperature and reorientation of the easy axis. At 77 K we observe 6% and 3% performance improvement of Gd and Dy poles as compared with V-P.

4. Discussion

4.1. Magnetic properties of re-crystallized rare-earth foils

Magnetic response of the a polycrystalline ferromagnetic material to the external magnetic field H is adequately described by Stoner-Wohlfarth [20] model, which assumes that orientation of a the magnetization vector M_s of a monodomain particle is determined by minimization of the following energy equation:

$$E = E_a + M_s H \cos\gamma - M_s^2 D_m \tag{1}$$

Here E_a is the magnetic anisotropy energy, γ is the angle between the magnetization vector and the external field and D_m is the demagnetization factor. The model does not take into account several factors, such as inter-particle coupling, however it can still be used to obtain an estimate of the saturation induction and permeability of a textured two-dimensional composite, such as a thin film [13] or, in this case, a foil. If the external field is directed away from the easy axis of the material, the M_s vector would acquire a position between the easy axis and the external field direction. The third term in Eq. 1 arises from the demagnetizing fields and imposes additional shape anisotropy.

In the following we will use the notation adopted by Rhyne and Clark [18] for the magnetic anisotropy energy of a hexagonal material:

$$E_a = K_2 P_2(\cos\theta) + K_4 P_4(\cos\theta) + K_6 P_6(\cos\theta) + K_6^6 \sin^6\theta \cos(6\phi) \tag{2}$$

Here, θ is the angle between the magnetization vector M and [0001] direction and ϕ is the angle between [1120] direction and the projection of M vector on (0001) plane, and P_m are Legendre polynomials of order m. For practical purposes, high-order terms K_4 and K_6 can be omitted. The anisotropy constants are very high, at 77 K K_2 = 4×10^7 J/m^3, K_6^6 = -1.4×10^5 J/m^3; at 4.2 K K_2 = 5.5×10^7 J/m^3, K_6^6 = -7.6×10^5 J/m^3 [18]. The magnetization curve analysis using Eq. 1 shows that in applied fields below 10 kOe the magnetic moment of a Dy domain is aligned along [1120] direction within 2°. Thus, magnetization of a textured sample is realized as 180° domain wall motion with no appreciable magnetic moment rotation. The saturation magnetization, achievable at <10 kOe can be calculated as the projection of $M_s \cos\gamma$. For (0001)[1010] oriented foils, synthesized by Swift et al. [21], the maximum magnetization is $M_s \cos(30°)$, or 86% of the theoretical value M_s. For the foils used in this study with domains oriented randomly within the (0001) plane, the magnetization moment is determined by the geometrical projections of M_s on the foil plane given random in-plane texture and a Gaussian distribution of the out-of-plane texture.

We modeled the saturation induction of a pole comprised of grains with (0001) texture but random basal orientation. The (0001) texture quality is defined as the width of the Gaussian distribution of the grains orientations with respect to the foil normal. For an ideally aligned foil the M_s value is 95% of the maximum, which is a significant improvement over (0001)[1010] texture value of 86%. Deterioration of the (0001) texture quality results in an expected reduction of M_s, however even a sample with relatively poor texture $\delta\theta = 20°$ would still have $M_s > 3$ T.

Besides M_s, the initial permeability μ_i is another critical factor which determines suitability of the pole material. Our simulation shows that it is desirable to have $\mu_i > 100$. Currently, μ_i of textured foils is in the range of 30 to 40, approximately two times lower than the optimum level. The low-field magnetization process is determined by motion of 180° domain walls. In the absence of the wall pinning, the domain wall motion is a fast low-energy process, which explains very high, over 1000, μ_i of single crystals. Relatively low μ_i of the foils indicate that some residual defects, such as strains and possibly oxide inclusions, impede the domain boundary motion. Further improvement of the annealing process is required to achieve the required μ_i value. The metallurgy guidelines developed for fcc metals indicate that the secondary recrystallization process becomes increasingly more effective at developing texture as the primary grain size decreases and the internal strain builds up [19]. Reducing the primary grain size can be accomplished by cold deformation, such as rolling or forging. In this case, a higher degree of thickness reduction by cold rolling would most likely be beneficial for the texture quality. The reduction of the foil thickness, however, has to be balanced against practical aspects of assembling a bulk pole from many very thin foils.

4.2. Application of the rare-earth poles for the storage ring undulators

In this section we will briefly discuss the value proposition of the rare-earth poles for storage ring undulators. The model undulator design has been derived from U-20 undulator, planned for the installation at NSLS-II storage ring. Fig. 11a shows schematic layout of the three magnet arrangements used in the analysis. In the modeling we use three permanent magnet arrangements: (1) a traditional 2D array with opposing permanent magnets; (2) 2D array with laterally magnetized side magnets; (3) added top magnets. The magnetization direction is schematically shown by white arrows. The magnetic field strength in the gap is increased as more flux is passed through a pole, however the gain in the gap field would be realized only if the pole is not saturated. The results presented in Fig. 11 were obtained using the code Radia [7], and based on the assumption of PrFeB permanent magnets with 1.5 T remanent magnetization (at 77 K) and a hypothetic non-linear isotropic (iron-type) magnetic material with saturation varying between 1T and 5T used for the poles. The ratio of the pole thickness to the half-period length was 0.3 in both undulator cases (i.e. no precise optimization was performed, but this parameter is reasonably close to the value used e.g. for the hybrid in-vacuum undulator U20 at NSLS-II).

Previous simulation had shown that the highest performance undulator can be had when the c-axis of the textured material is defined along the transverse direction of the undulator (the direction of electron undulation). Orienting the c-axis along the longitudinal dimension, that is the direction that the electron beam principally travels, decreases the peak undulator field by a few percent, while orienting the c-axis in the vertical direction significantly degraded undulator performance. However, the anisotropy of the textured dysprosium material was not taken into account in the simulations illustrated in Fig. 11. Taking into account the anisotropy will eventually make the performance gain lower.

To find limits imposed by the pole material we simulated the three geometries shown in Fig. 11a using a model pole material with variable saturation inductance. In the simulations the pole material is modeled as a soft ferromagnet with the initial magnetic permeability $\mu_i = 1000$ and variable saturation inductance M_s, which is changed from 1 to 5 T. Fig. 11b shows dependence of the peak magnetic field as a function of M_s of the pole. The vertical lines correspond to the saturation inductance of V-P, 2.3 T, and Dy, 3.5 T. The simulation curves exhibit initial linear dependence of B_g on M_s. In this regime the maximum gap field changes little as the extra permanent magnets are added to the array, since the pole is fully saturated and cannot utilize the extra magnetic field strength. For this reason an undulator with V-P poles would have practically the same performance for the three geometries shown in Fig. 11a.

A plateau at $M_s = 3$ T indicates that the pole cannot be saturated by the 2D permanent magnet array. In this regime the added complexity of (b) and (c) geometries pays off as an approximately 20% enhancement of the gap field, consistent between the optimized 17 mm period design and the 13 mm unoptimized design. The second vertical line shows that textured Dy is well position to take an advantage of the higher magnetic field strength created by the complex permanent magnet arrays. Such designs make use of more magnet material per period of undulator as well as using a higher cost pole material, however, the field enhancement may be worth the extra cost for facilities which have limited space for insertion devices such as lower energy synchrotrons or free-electron lasers that require expensive tunnel space.

5. Conclusions

In conclusion, we investigated feasibility of using dysprosium and gadolinium metals as a pole material in short period cryo-cooled undulator. Rolling-induced texturing has been employed to align the easy magnetization plane of the pole with the magnetic field direction. We observed 3- 6% enhancement of the axial gap field at 77 K when the Vanadium-Permendur poles were replaced with textured dysprosium or gadolinium poles. The future work is focused on validation the new pole performance at 30 K, where Pr-Nd-Fe-B magnets have the highest remnant induction and the rare earth poles are expected to deliver higher magnetization. In addition, the factor of 10 increase in thermal conductivity of copper at 30 K as compared to 300 K is expected to decrease thermal gradients along long undulator structures. While the textured foils demonstrate the saturation inductance values comparable to single crystals, further improvements of the permeability are required to realize the full potential of rare-earth metals for undulator applications.

[1] D. Barlow, R.K. Jr., C. Lobb, M. Menzel, P. Walstrom, Nuclear Instruments and Methods in Physics Research Section A: Accelerators, Spectrometers, Detectors and Associated Equipment 313 (1992) 311 – 314.

[2] D.R. Behrendt, S. Legvold, F.H. Spedding, Phys. Rev. 109 (1958) 1544–1547.

[3] C. Benabderrahmane, P. Berteaud, M. Vallau, C. Kitegi, K. Tavakoli, N. Bechu, A. Mary, J. Filhol, M. Couprie, Nuclear Instruments and Methods in Physics Research Section A: Accelerators, Spectrometers, Detectors and Associated Equipment 669 (2012) 1 – 6.

[4] M. Bird, S. Bole, I. Dixon, Y. Eyssa, B. Gao, H. Schneider-Muntau, Physica B: Condensed Matter 294295 (2001) 639 – 642. Proceedings of the Sixth International Symposium on Research in High Magnetic Fields.

[5] C.W. Chen, Journal of Applied Physics 32 (1961) S348–S355.

[6] A.S. Chernyshov, A.O. Tsokol, A.M. Tishin, K.A. Gschneidner, V.K. Pecharsky, Phys. Rev. B 71 (2005) 184410.

[7] O. Chubar, P. Elleaume, J. Chavanne, J. Synchrotron Rad (1998). 5, 481-484 (1998) 1–4.

[8] S. Gottschalk, A. Pindroh, D. Quimby, K. Robinson, J. Slater, Nuclear Instruments and Methods in Physics Research Section A: Accelerators, Spectrometers, Detectors and Associated Equipment 304 (1991) 732 – 737.

[9] K. Halbach, Nuclear Instruments and Methods inPhysics Research, Section A 187 (1981) 109–117.

[10] T. Hara, T. Tanaka, H. Kitamura, T. Bizen, X. Maréchal, T. Seike, T. Kohda, Y. Matsuura, Phys. Rev. ST Accel. Beams 7 (2004) 050702.

[11] J.F. Herbst, Reviews of Modern Physics 63 (1991) 819–898.

[12] F. Humphreys, Recrystallization and Related Annealing Phenomena, Elsevier Science, 1995.

[13] B. Jamieson, T. O'Donnell, S. Kulkarni, S. Roy, Applied Physics Letters 96 (2010) 202509.

[14] J. Jensen, A. Mackintosh, Rare earth magnetism: structures and excitations, International series of monographs on physics, Clarendon Press, 1991.

[15] D. Larbalestier, A. Gurevich, D.M. Feldmann, A. Polyanskii, Nature 414 (2001) 368.

[16] S. Mishra, C. Drmann, K. Lcke, Acta Metallurgica 32 (1984) 2185 – 2201.

[17] F.H. O'Shea, G. Marcus, J.B. Rosenzweig, M. Scheer, J. Bahrdt, R. Weingartner, A. Gaupp, F. Grüner, Phys. Rev. ST Accel. Beams 13 (2010) 070702.

[18] J.J. Rhyne, A.E. Clark, Journal of Applied Physics 38 (1967) 1379–1380.

[19] A. Rollett, W. Mullins, Scripta Materialia 36 (1997) 975 – 980.

[20] E.C. Stoner, E.P. Wohlfarth, Philosophical Transactions of the Royal Society of London. Series A, Mathematical and Physical Sciences 240 (1948) 599–642.

[21] W. Swift, M. Mathur, IEEE Transactions on Magnetics 10 (1974) 308–313.

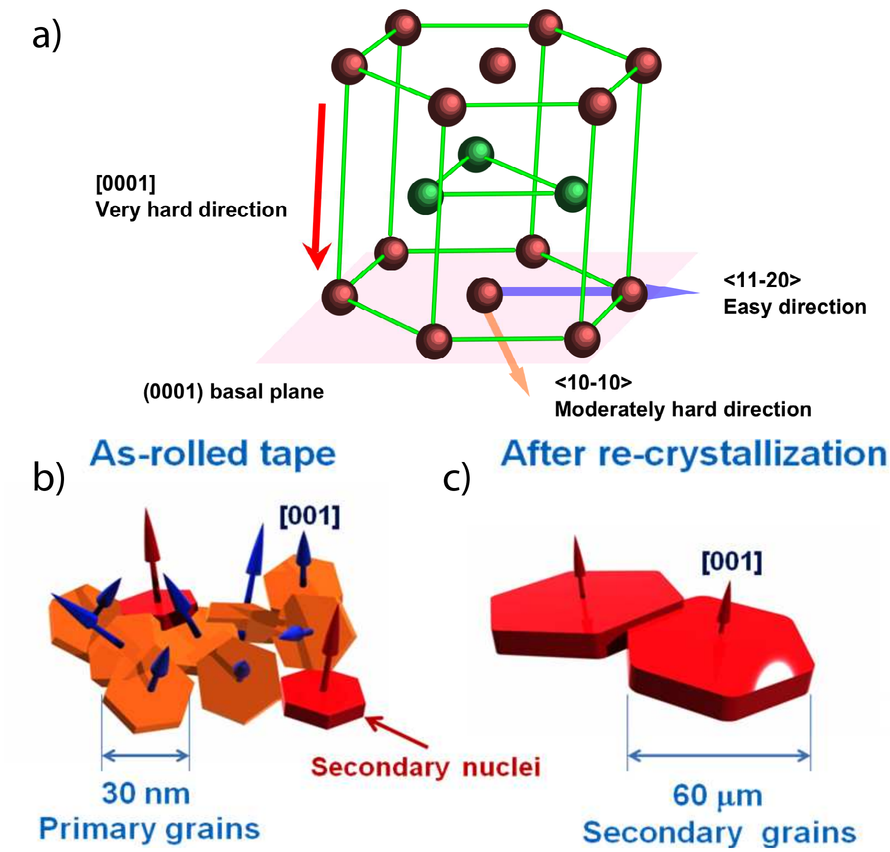

Figure 1: a) Crystal structure of Dy metal showing principal magnetization directions. b), c) Schematic illustration of the secondary re-crystallization process: better oriented primary grains become nuclei of large secondary grains consuming mis-oriented primary grains (panel b). This results in quasi-crystalline structure of the re-crystallized tape (panel c).

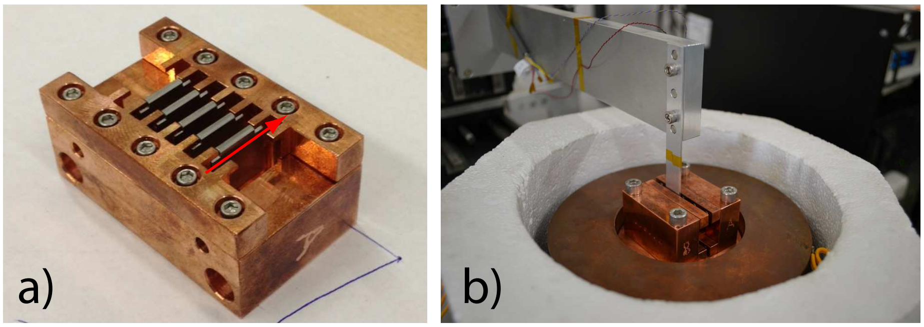

Figure 2: a) Partially assembled test undulator array without magnets, the c-axis of the textured dysprosium is oriented along the direction shown by the red arrow. The poles are numbered 1 through 5 starting on the left of the image. b) Cryogenic setup for magnetic field measurement.

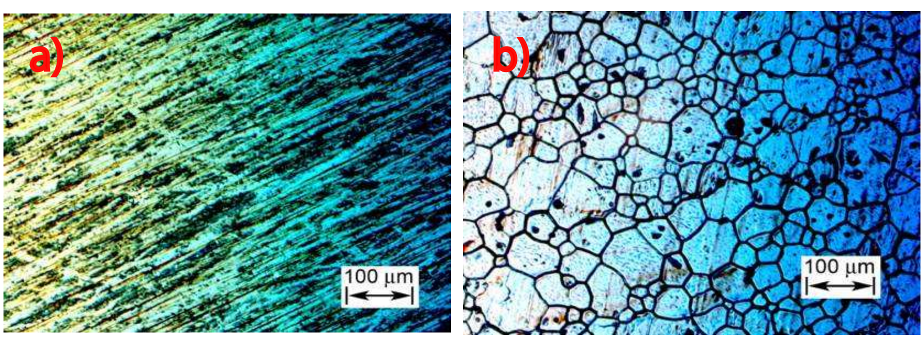

Figure 3: a) Optical surface micrograph of as-rolled 60 μm Dy foil, b) and effect of 10 min annealing at 1100°C: bright-field micrograph. Note formation of large secondary grains.

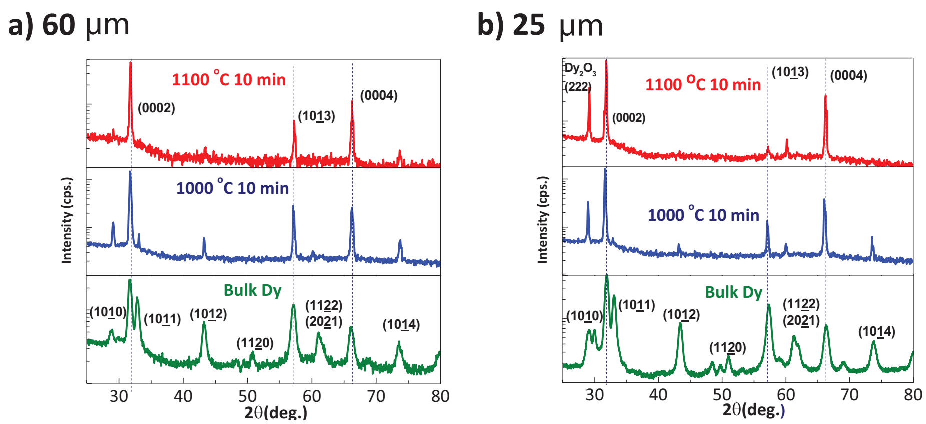

Figure 4: X-ray diffraction 2θ scans of 60 μm (panel a) and 25 μm (panel b) Dy foils: as-rolled and after 10 min of annealing at 1000°C and 1100°C. Note strong (000l) texture of 25 μm foil after 10 min annealing at 1100°C; 60 μm foil shows residual grains with (1013) orientation after the same processing. Surface oxidation is detectable as (222) Dy_2O_3 peak. The development of texture is due to the combination of large compression ratio during rolling and the annealing.

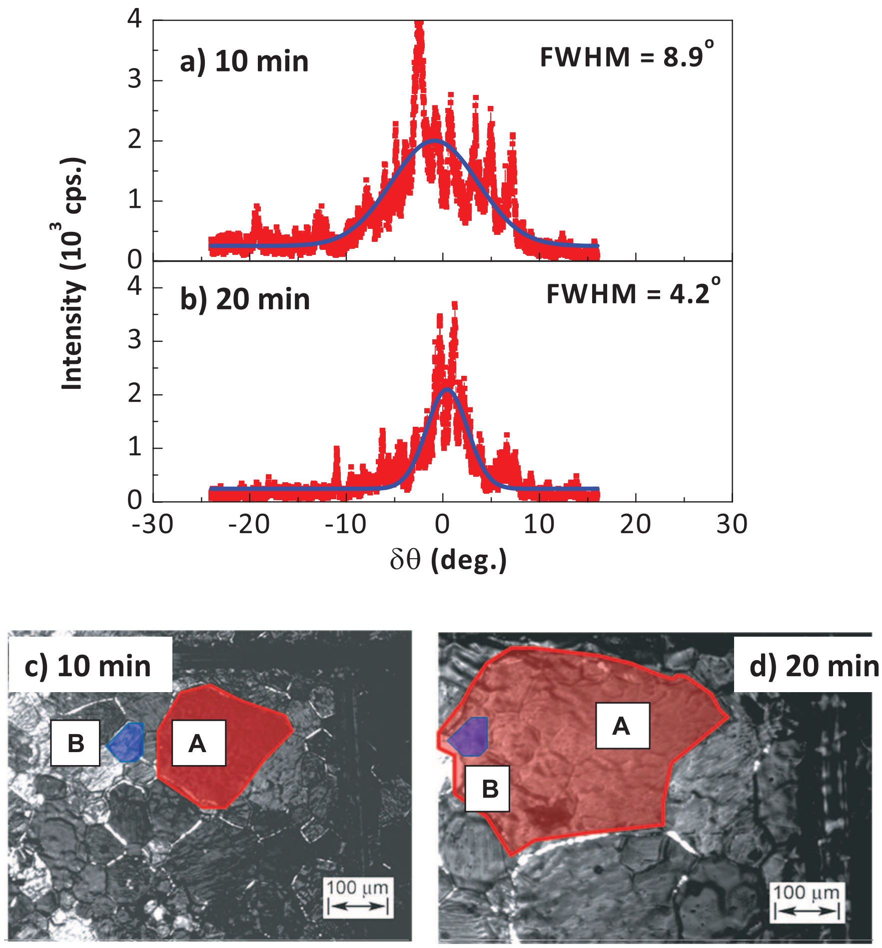

Figure 5: a) Rocking curves of (0004) Dy reflection showing improvement of out-of plane texture of 25 μm foils after longer annealing at 1100°C. The out-of-plane texture saturated at approximately 4° level after 15 min of annealing at 1100°C (b). Solid lines are Gaussian approximations, FWHM value is calculated from the approximation. c and d) Same area optical micrographs showing expansion of abnormal (0001) grain after 10 min (panel c) and 20 min of annealing (panel d) of 25 μm thick foil at 1100°C. The process of better oriented secondary grain expansion explains the texture improvement shown in panels a and b.

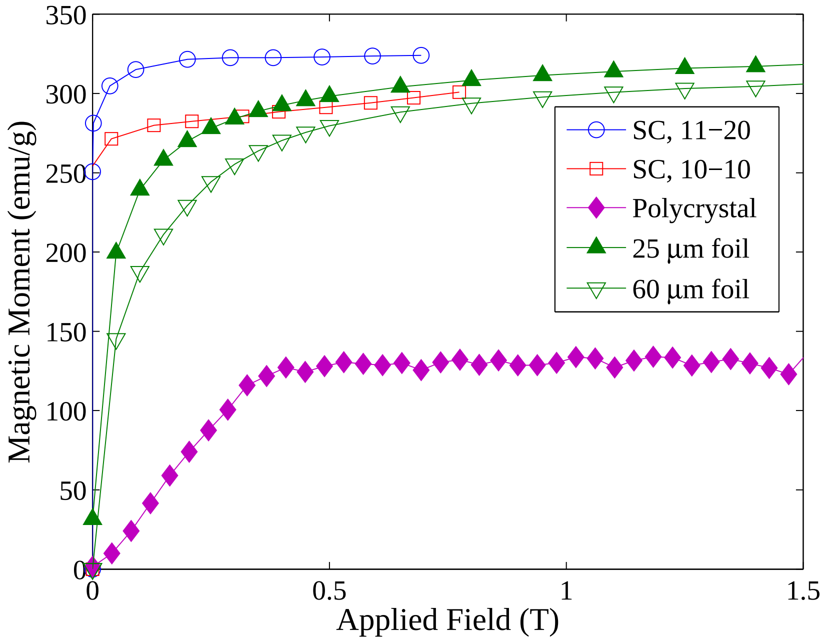

Figure 6: Magnetization curves of polycrystalline Dy, a single crystal (SC) and textured foils at 77 K. The single crystal data are adopted from Behrendt *et al.* [2].

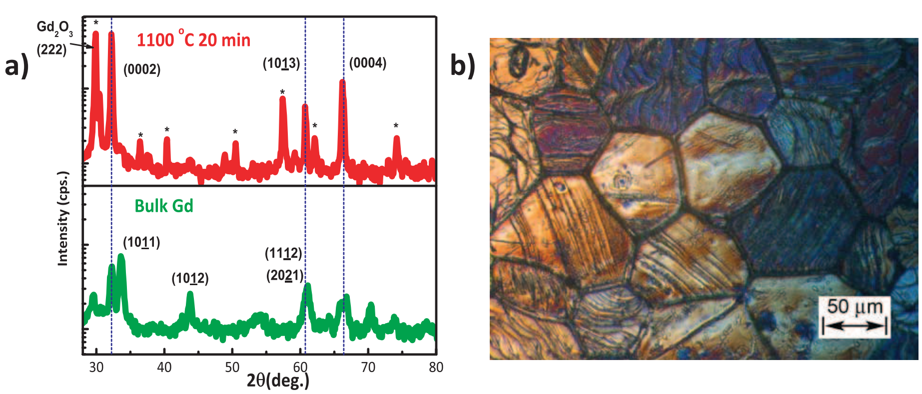

Figure 7: a) X-ray diffraction 2θ scans of 100 μm rolled Gd foil before (lower plot) and after (upper plot) of heat annealing at 1100°C for 20 min. b) Optical micrograph of textured Gd foil. Similar to Dy foil, Fig. 3, we observe well-defined large secondary grains. Peaks corresponding to cubic Gd_2O_3 phase are labeled with a '*' symbol.

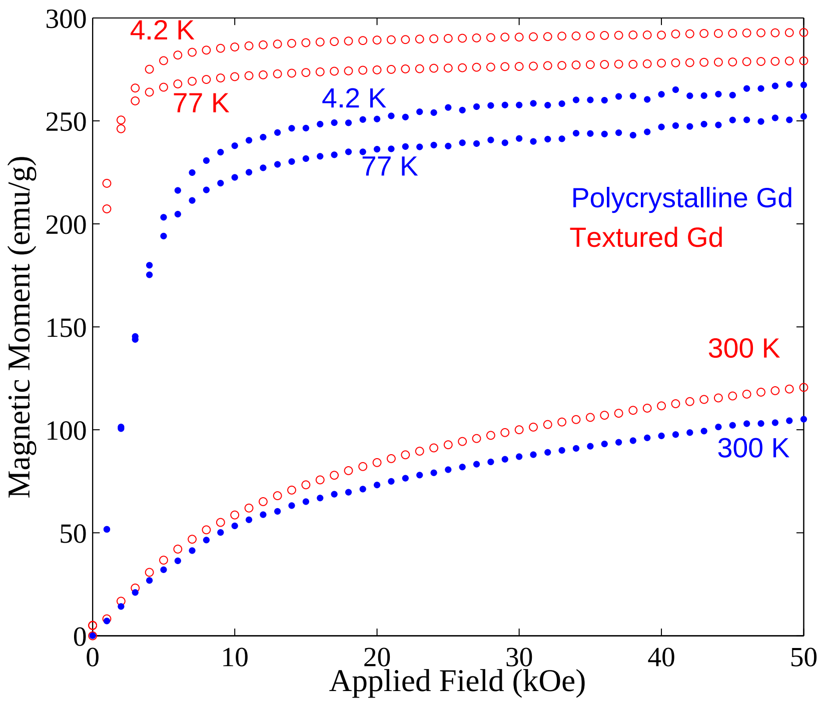

Figure 8: Magnetization curves of a polycrystalline Gd sample (filled blue circles) and a textured 100 μm Gd foil (open red circles) at 300 K, 77 K and 4.2 K.

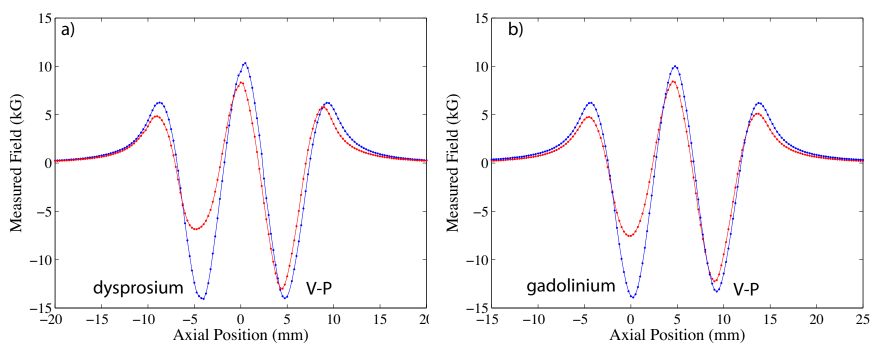

Figure 9: Scans of the gap field of the test undulator with Dy poles (a) and Gd poles (b). In both images the blue curve is the measurement at 80 K and the red curve is the measurement at room temperature.

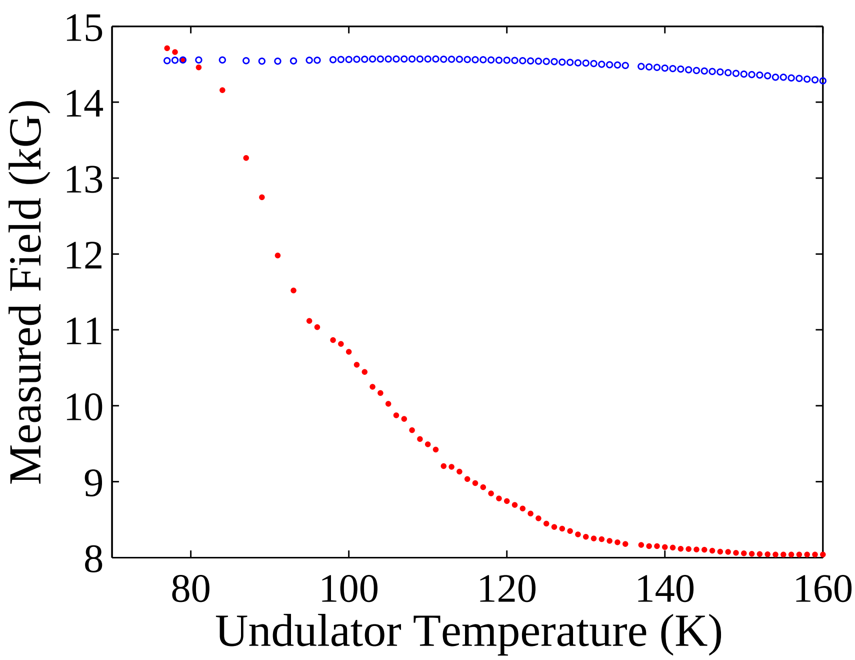

Figure 10: Temperature dependence of the field of the undulator between Dy poles (red dots) and Vanadium-Permendur pole (blue circles). The Dy pole outperforms the Vanadium-Permendur for temperatures below 80 K.

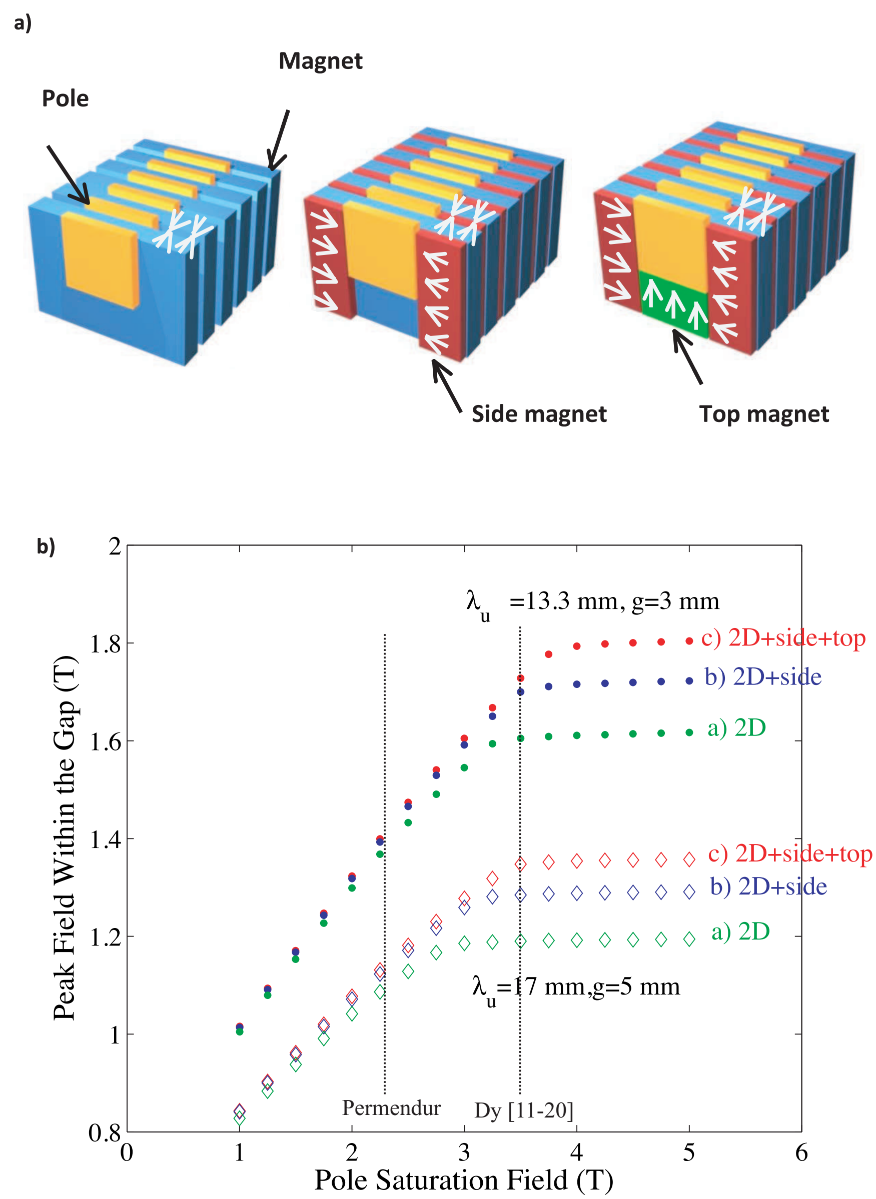

Figure 11: a) Schematic layout of the three magnet array geometries used in the analysis. The three permanent magnet array geometries differ by extra magnet inserts with sideways, and vertical magnetization. The arrows indicate direction of magnetization in the permanent magnets. b) Gap field of U-20 undulator as a function of the saturation inductance, M_s, of the pole for the three magnet array configurations shown in panel a). The vertical lines represent M_s values for Vanadium Permendur (2.3 T) and Dysprosium (3.5 Tesla at 77 K).